IET Control Theory & Applications

Research Article

IET Journals
The Institution of Engineering and Technology

Induction machines sensors-less wind generator with integrated intelligent maximum power point tracking and electric losses minimisation technique

ISSN 1751-8644
Received on 1st October 2014
Revised on 5th March 2015
Accepted on 31st March 2015
doi: 10.1049/iet-cta.2014.1049
www.ietdl.org

Marcello Pucci ✉

Institute of Intelligent Systems for the Automation (ISSIA), National Research Council of Italy (CNR), Palermo, Via Dante, 12 90100 Palermo, Italy
✉ *E-mail: pucci@pa.issia.cnr.it*

Abstract: This study presents a high-performance wind generation system with induction machine (IM), specifically devised with the target of maximising the efficiency of the electromechanical conversion, and contemporary minimising the number of the system sensors and their cost. To this aim, the control system has been integrated, from one side, with an intelligent maximum power point tracking (MPPT) technique, so to make the generator track the power available in the wind, from the other side with techniques for the minimisation of the electrical losses (ELMT). Particularly, the power converters' switching losses have been reduced adopting a discontinuous pulsewidth modulation, while the IM overall losses have been reduced by a suitable electric losses minimisation technique. Contemporary, to reduce costs and increase the reliability of the system, the system has been devised as a fully sensors-less generation unit, meaning that both the wind speed and the machine speed sensors are not present. The anemometer has been substituted by the wind speed estimator integrated in the MPPT, based on the growing neural gas (GNG) network. The encoder has been substituted with an intelligent IM speed estimator, the so called MCA EXIN + reduced order observer (ROO). The performance of the adopted technique has been verified experimentally on a suitably devised test set-up.

1 Introduction

Nowadays, wind energy is becoming an ever more exploited renewable energy source [1, 2]. Modern solutions range from permanent magnet synchronous machines, to doubly-fed induction machine or squirrel cage induction machine (IM), each supplied by a suitable power converter [3, 4]. Whatever is the machine chosen, from the control point of view, the most challenging issues to be solved are described in the following.

First, suitable maximum power point techniques (MPPT) should be developed, able to quickly track any variation of the wind speed, and correspondingly of its power, inside the variable speed range of the wind turbine, avoiding perturb and observer (P&O) [5–7] or hill and climb (H&C) algorithms, inevitably requiring very long times to converge in systems characterised by high inertias, as wind generators typically are, and causing persistent undesired oscillations around the MPPs. Even other methods, for example those exploiting proper wind turbine modelling [8–11] to compute the optimal power reference speed of the drive, can be problematic since they often require the knowledge of a wind speed sensor to work, whose presence can significantly increase the cost and reduce the reliability of the drive system, Some intelligent neural based MPPTs have been proposed in [12, 13], respectively, adopting a two radial basis function NNs and a multi-layer perceptron trained by a back-propagation (BPN) algorithm as a virtual anemometer. Both these approaches present the following significant drawbacks: (1) with such approaches, no evidence of the correct learning of inverse characteristic of the wind turbine exists and, (2) a very complex and computational demanding structure of the MLP (100 neurons in the hidden layer) is needed. Finally, no experimental evidence of the correct behaviour of the MPPT has been provided in both works.

Second, the control system should be integrated with techniques permitting the maximisation of the efficiency of the electric conversion chain, by the reduction of its losses. From this point of view, electric losses are concentrated in both the power converters and the electrical machine. The main power converters' losses terms are switching and conduction ones. The latter can be significantly reduced, once the switching frequency of the converter is fixed, by adopting suitable pulsewidth modulation (PWM) techniques, such as the discontinuous (D-PWM) ones [14–16]. The electric generator losses terms depend on the kind of machine, and correspondingly any electrical loss minimisation technique (ELMT) [17–19] does. All of these techniques are based on the idea of reducing the magnetisation of the machine by directly acting either on the reference flux or on the direct component of the stator current in the field reference frame, for lower values of the load torque.

Third, if the generator power is supposed to be controlled acting on its reference speed, a speed sensor is required to close the speed control loop. The presence of this sensor increases the cost of the wind plant and reduces its reliability, especially in high power units. This is the reason why sensorless techniques to be integrated in the machine control reveal very interesting for such an application. The scientific literature dealing with sensorless techniques is huge [20–22], ranging from high frequency rotating or pulsating voltage injection, to the adoption of test vector, to the adoption of model based techniques. Since the wind generator is supposed to work tracking the maximum available power, in a wide speed range, from the rated to low speed (hardly zero speed, because the generator is characterised by a cut-in working speed), model based sensorless techniques reveal more suitable for such an application.

This paper presents a high performance wind generation system with IM, specifically devised with the target of maximising the efficiency of the electromechanical conversion and contemporary minimising the number and cost of the system sensors. To this aim, the control system has been integrated, from one side, with an intelligent MPPT technique, hence to make the generator track the power available in the wind, from the other side with techniques for the minimisation of the electrical losses. Particularly, the power converters' switching losses have been reduced adopting a

particular kind of D-PWM, the so called D-PWMmax [15]. The IM losses have been minimised, adopting an improved version of the ELMT proposed in [35], modified to be implemented in terms of the rotor flux reference instead of the direct component of the stator current reference. Contemporary, to reduce costs and increase the reliability of the system, the system has been devised as a fully sensors-less generation unit, meaning that both the wind speed and the machine speed sensors are not present. The anemometer has been substituted by the wind speed estimator integrated in the MPPT, based on the growing neural gas (GNG) network. The encoder has been substituted with an intelligent IM speed estimator, the so called MCA EXIN + reduced order observer (ROO) [23]. The adopted MPPT, initially proposed in [24], upgraded in [25] with a total least-squares (TLS) EXIN full order Luenberger observer speed observer and in [26] with a MCA EXIN + ROO speed observer, has been here further upgraded hence to cover a wider wind speed range. The MPPT is based on a particularly kind of self-supervising neural network, called GNG, presenting the capability to deal with function discontinuities and to invert functions, where invertible. The proposed intelligent control technique applied to the wind generator is an upgrade of that proposed in [26], with respect to which the main differences here are the integration in the control system of the D-PWM and the ELMT features. The entire IM-based wind generation unit with integrated MPPT, ELMT, D-PWM and sensorless features has been tested experimentally on a suitably developed test set-up. The improvements in terms of power and energy transferable to the power grid with respect to the [26] are shown as well.

2 Wind turbine model

This section briefly describes the adopted model of the wind turbine. The power generated by a wind turbine can be written as:

$$P_{\mathrm{m}} = C_{\mathrm{p}}(\lambda, \beta)\frac{\rho A}{2}v^3 \tag{1}$$

where P_{m} is the mechanical power of the turbine in [W], C_{p} is the power coefficient of the turbine, ρ is the air density in [kg/m^3], A is the turbine swept area in [m^3], v is the wind speed in [m/s], λ is the tip speed ratio, β is the blade pitch angle in [deg]. For the expression of the function C_{p} (λ) see [23]. The tip speed ratio λ is defined on the basis of this expression: $\lambda = \omega_{\mathrm{T}}R/v$, where ω_{T} is the turbine angular speed. The torque produced by the turbine can be computed as

$$T_{\mathrm{T}} = P_{\mathrm{m}}/\omega_{\mathrm{T}} = C_{\mathrm{T}}(\lambda, \beta)\frac{\rho\,\pi\,R^3}{2}v^2 \tag{2}$$

where the torque coefficient of the turbine is defined as $C_{\mathrm{T}}(\lambda, \beta) = C_{\mathrm{P}}(\lambda, \beta)/\lambda$. The adopted turbine model parameters are shown in Table 1.

Table 1 Wind turbine parameters

R, m	2.5
λ_{opt}	7
C_{pmax}	0.45
n	4.86
generator rated power, kW	5.5
generator rated speed, rpm	1500

3 Control technique

The control system of the proposed wind generator is composed of four separate control systems: (1) a field oriented control (FOC) for the induction generator (Fig. 1), (2) a voltage oriented control (VOC) for the grid-connected inverter, (3) an MPPT algorithm for tracking the maximum generable power from the wind, (4) an ELMT algorithm for minimising the power losses in the IM. The complete wind generator control scheme is sketched in Fig. 1.

3.1 Field oriented control

The IM side converter has been controlled by the so called FOC (Fig. 1).

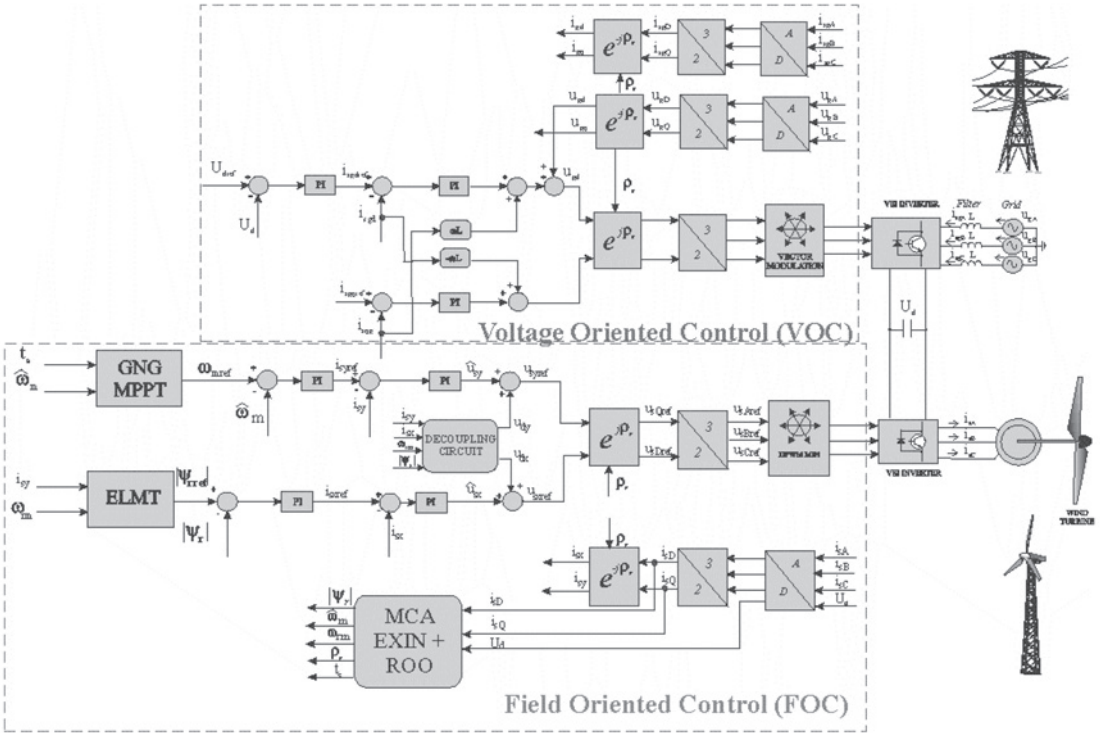

Fig. 1 *Block diagram of the wind generator control scheme*

IET Control Theory Appl., 2015, Vol. 9, Iss. 12, pp. 1831–1838

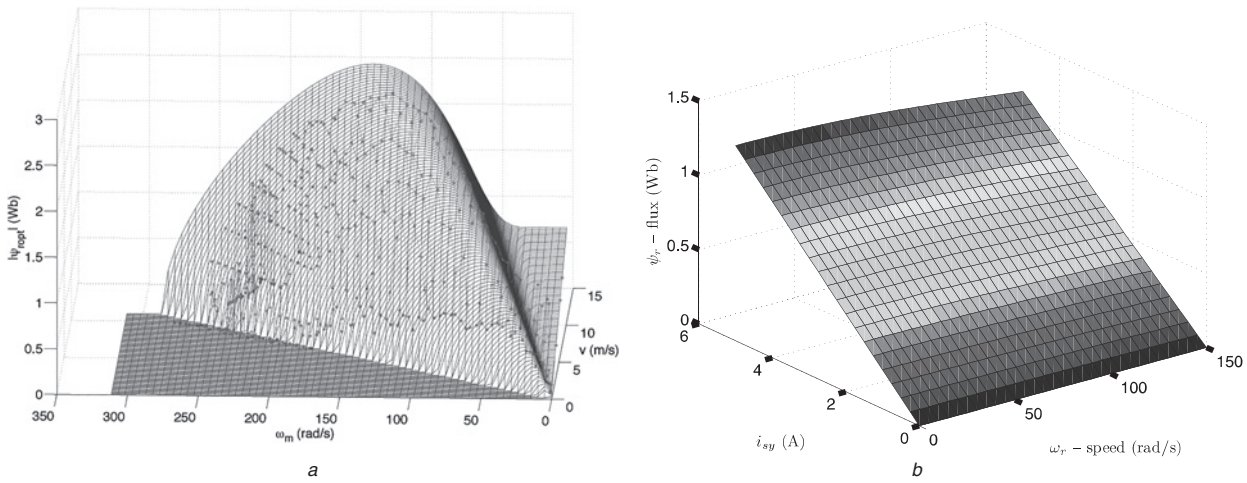

Fig. 2 *MPPT-ELMT control surfaces*

a Distribution of the neurons and links of GNG on the wind turbine surface (left-hand side)
b ELMT surface characteristic (right-hand side)

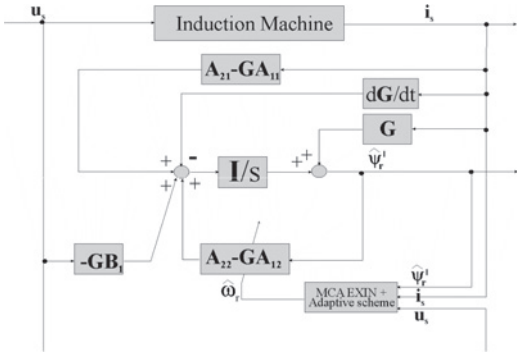

Fig. 3 *Block diagram of the MCA EXIN + reduced order speed observer*

The DC-link voltage is assumed to be constant, since its control is performed by the grid side inverter. On the direct axis (x-axis), a flux control loop commands the current loop. The rotor flux linkage amplitude reference ψ_{rref} is provided by the ELMT block, receiving in input the actual values of the quadrature component of the stator current in the field reference frame i_{sy} as well as the actual value of the supply pulsation ω_{rm}, obtained by the MCA EXIN + ROO as the instantaneous value of the angular speed of the rotor flux linkage space vector. On the quadrature axis (y-axis), a speed loop controls the current loop (Fig. 3). The reference speed of the generator ω_{mref} is provided by the GNG MPPT, receiving in input the current values of the IM torque t_e and speed ω_{m}. The speed needed to close the speed loop is provided by the MCA EXIN + ROO.

It should be noted that the flux and speed control loops are inherently coupled by the contemporary presence of the MPPT, ELMT and sensorless algorithms. This makes the overall coordination of the entire control system very challenging. As a matter of fact, any speed variation imposed by the MPPT implies a turbine torque variation, with consequent IM losses variation leading to reference flux variation imposed by the ELMT to minimise the IM losses. The control coordination is further complicated by the fact that the IM speed is not measured, while it is estimated by the MCA EXIN + ROO; the real electromechanical dynamics and the estimated one can thus be quite different. For this reason, since the MTTP and the ELMT should work contemporary, their reciprocal dynamics has to be be carefully tuned considering the dynamics of the MCA EXIN + ROO; this last dynamics must be selected to reproduce at the best the IM mechanical dynamics, in the widest speed range as possible. In the case under study, the ELMT does not introduce any dynamics, since it is based on a static mapping. With regard to the MPPT, neither the GNG network implies any dynamics. Its dynamics is governed by the 1st order low pass filter at the output of the GNG. The pole of such a filter is usually chosen [24, 25] hence to guarantee the stability of the speed control loop and, in any case, coherently with the inertia of the wind turbine. On this basis, the speed loop reference variation is much slower than the flux reference variation, because of both the first order lag at the end of the MPPT and the MCA EXIN + ROO, guaranteeing that the IM is, in each instant, correctly magnetised according to the ELMT independently from the current value of the machine speed, imposed by the MPPT.

3.2 Discontinuous-pulsewidth modulation

D-PWM is also called two-phase SV-PWM. It is a particular kind of carrier based technique, where the zero sequence signals is added in such a way that only two phases of the VSI are switched at the same time [1, 22]. Each phase is clamped either to the upper or to the lower DC-link bus for a certain angle of 60° or 120°. Among the several D-PWM techniques, the D-PWMmax has been chosen for driving both the IM and grid side VSIs.

In the case under study, during the modulation time T_{PWM} the expression of the duty cycle of the n-phase leg is

$$\delta_{sn} = \frac{1}{2} + \frac{u_{sn\text{ref}} + u_0}{U_{\text{d}}} \tag{3}$$

where $u_{sn\text{ref}}$ ($u_{sn\text{ref}} = u_{sA\text{ref}}, u_{sB\text{ref}}, u_{sC\text{ref}}$) is the amplitude of the sinusoidal reference voltage of the phase n, U_{d} is the DC-link voltage and u_0 is a zero-sequence signal, equal in this case to

$$u_0 = \frac{U_d}{2} - \max_n(u_{sn\text{ref}}) \tag{4}$$

For the experimental implementation of the D-PWMmax, a PWM frequency of $f_{\text{PWM}} = 5$ kHz has been used to command both VSIs. The sampling frequency of the entire control system has been set to 10 kHz.

4 GNG-based MPPT

The adopted MPPT technique is based on that proposed in [24], improved and retuned here to increase the accuracy of the wind speed estimation and to enlarge the wind speed range in which the technique properly works.

The target of MPPT is to make the machine work at the speed corresponding to the maximum power extractable from the wind turbine. In this case, the generator reference speed ω_{mref} can be

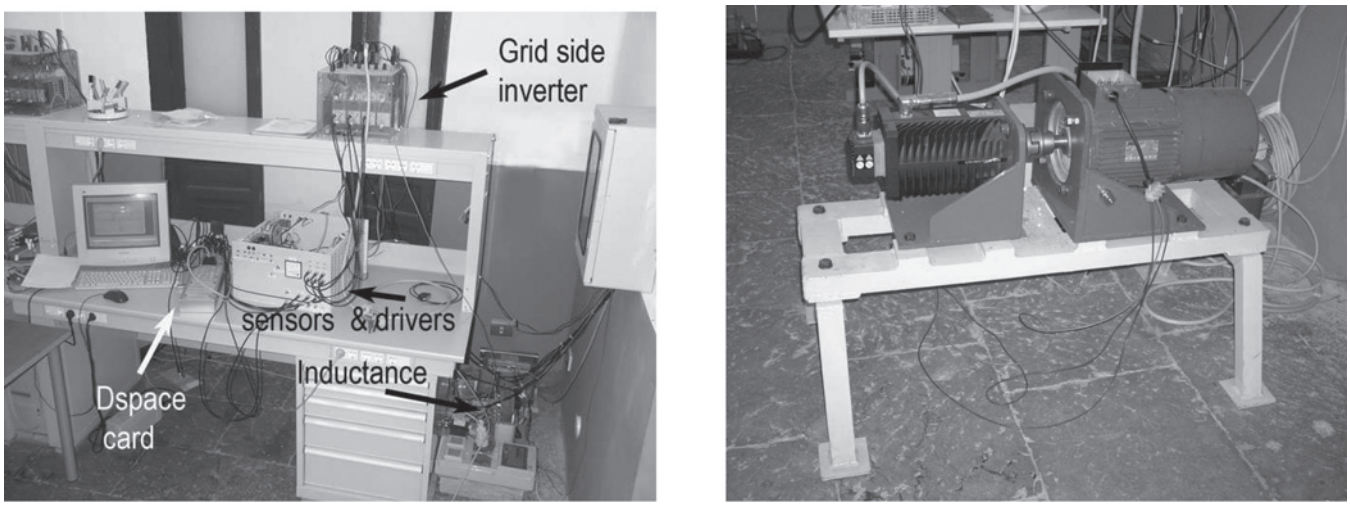

Fig. 4 *Photograph of the test setup*

a Test setup (left-hand side)
b Induction generator + turbine emulator (right-hand side)

computed on the basis of the following expression

$$\omega_{\text{mref}} = n\, v_{\text{stim}}\, \lambda_{\text{opt}}/R \tag{5}$$

where λ_{opt} is the optimal value of the tip speed ratio, which is a known quantity and depending on the characteristics of the turbine, v_{stim} is the estimated wind speed. For stability reasons, the optimal generator reference speed is not directly provided to the machine control system, but is filtered by a first order filter with time constant τ to avoid instability phenomena of the whole control system, as explained in [24].

The turbine model described in Section 2 has been generated off-line to create the complete training set of data, characterising the direct function of the wind turbine. This relationship has been then learnt off-line by a GNG network developed by the authors in Matlab®-Simulink® environment (for the description of the adopted GNG algorithm see [24]). A GNG with a maximum number of 800 neurons has been used, that does not imply a significant computational burden, since it requires only a storage of a 800×3 matrix in the memory of the DSP. After training, the GNG has been used on-line by exploiting the turbine characteristic function to be inverted. It should be noted that the function inversion capability is one of the key issues by which this neural network is suitable for this application, whereas the classic MLP trained by the back-propagation is not able to perform this task. Fig. 2a shows the surface describing the direct characteristic of the wind turbine, expressing the relationship between the turbine torque, reported to the IM level t_e, against the IM speed ω_{m} and wind speed v. It further draws the neurons created by the GNG with the corresponding links after training, as well as the curve connoting the maximum power points (MPPs). This figure clearly shows that the neurons created by the GNG properly cover the turbine characteristic, representing the topological disposition of the data. The links among the neurons show how data have been connected during the training process.

5 Electrical losses minimisation technique

The ELMT adopted in this wind generator system is basically that proposed in [19], improved here expressing the regulation variable in terms of the rotor flux reference, instead of the direct component of the stator current in the rotor flux oriented reference frame to make it more compatible with the adopted version of FOC.

The overall active power lost during the regular operation of the IM can be expressed as

$$P_{\text{loss}} = a i_{sx}^2 + b i_{sy}^2 \tag{6}$$

The a and b terms can be obtained as

$$\begin{aligned} a &= 3R_{\text{s}} + c_{\text{Fe}}\omega_e^2 L_m^2 \\ b &= \left(3R_{\text{s}} + 3R_{\text{r}}\frac{L_{\text{m}}^2}{L_{\text{r}}^2}\right) + \left[c_{\text{Fe}}\left(L_{\text{m}} - \frac{L_{\text{m}}^2}{L_{\text{r}}}\right)^2 + c_{\text{str}}\frac{L_{\text{m}}^2}{L_{\text{r}}^2}\right]\omega_e^2 \end{aligned} \tag{7}$$

where c_{Fe} and c_{str} are the iron and stray losses coefficients, respectively.

To achieve the minimum value of electric loss, assuming that both the electromagnetic torque t_e and the supply pulsation ω_e are constant, it should be verified that: $\left.\frac{\partial P_{\text{loss}}}{\partial i_{sx}}\right|_{\omega_e = k} = 0$.

It can be finally found that the optimal value of ψ_{rrefopt}, that minimise the electrical loss, can be obtained as

$$\psi_{\text{rrefopt}} = L_{\text{m}}|i_{sy}|G_{\text{d}}\sqrt{\frac{1 + T_a^2\omega_e^2}{1 + T_b^2\omega_e^2}} \tag{8}$$

where

$$\begin{aligned} G_{\text{d}} &= \sqrt{1 + \frac{R_{\text{r}}L_{\text{m}}^2}{R_{\text{s}}L_{\text{r}}^2}} \\ T_a &= L_{\text{m}}\sqrt{\frac{c_{\text{Fe}}(L_{\text{r}} - L_{\text{m}})^2 + c_{\text{str}}}{3(R_{\text{s}}L_{\text{r}}^2 + R_{\text{r}}L_{\text{m}}^2)}} \\ T_b &= L_{\text{m}}\sqrt{\frac{c_{\text{Fe}}}{3R_{\text{s}}}} \end{aligned} \tag{9}$$

Fig. 2b shows the minimum losses control surface, describing the function $|\boldsymbol{\psi}_{\text{rref}}| = f(i_{sy}, \omega_e)$, as implemented in the experimental set-up. As for ω_e to be used in the minimum losses algorithm, the angular speed of the rotor flux linkage space vector ω_{rm} has been obtained as the sum between the rotor speed and the slip speed, taken from the MCA EXIN + ROO block in Fig. 1.

6 MCA EXIN + ROO

To reduce the cost and increase the reliability of the wind generation system drive, the IM speed of the IM needed for closing the speed loop, has been estimated by the MCA EXIN + ROO, whose theoretical properties and experimental performance have been fully demonstrated [23] in case of a motor drive application, and adopted in [26] in a wind generation unit. In the following it has been only briefly explained, for the sake of readability.

IET Control Theory Appl., 2015, Vol. 9, Iss. 12, pp. 1831–1838

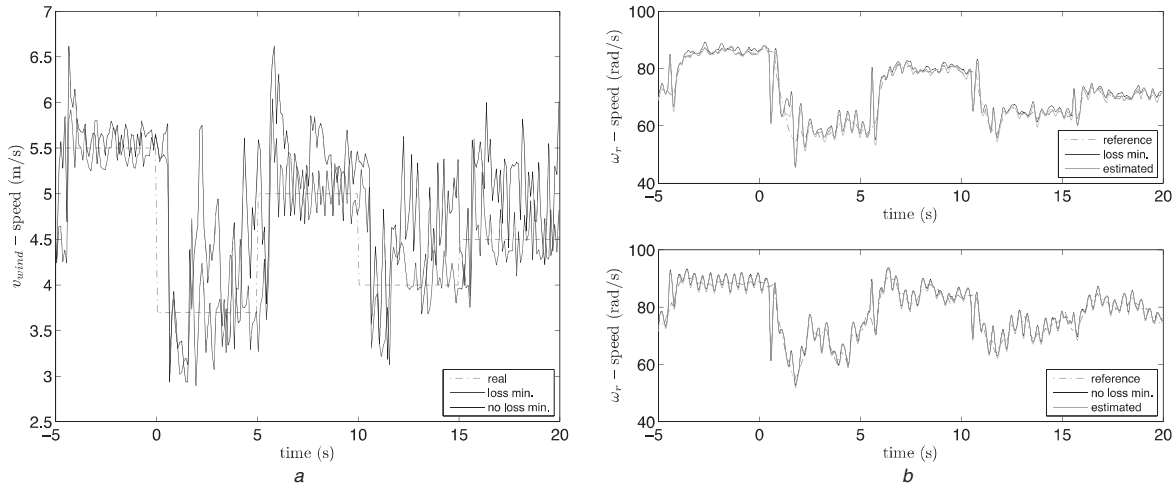

Fig. 5 *Minimum losses control surface*

a Real and estimated wind speed, with GNG MPPT, with and without ELMT (left-hand side)
b Reference and measured estimated machine speed, with and without ELMT (right-hand side)

6.1 Reduced order observer

The reduced order state observer estimating the rotor flux linkage of the IM is given as usual by

$$\frac{\mathrm{d}}{\mathrm{d}t}\hat{\boldsymbol{\psi}}_{\boldsymbol{r}}' = \boldsymbol{A}_{22}\hat{\boldsymbol{\psi}}_{\boldsymbol{r}}' + \boldsymbol{A}_{21}\boldsymbol{i}_{\boldsymbol{s}} + \boldsymbol{G}\left(\frac{\mathrm{d}}{\mathrm{d}t}\boldsymbol{i}_{\boldsymbol{s}} - \boldsymbol{A}_{12}\hat{\boldsymbol{\psi}}_{\boldsymbol{r}}' - \boldsymbol{A}_{11}\boldsymbol{i}_{\boldsymbol{s}} - \boldsymbol{B}_1\boldsymbol{u}_{\boldsymbol{s}}\right)$$
$$= (\boldsymbol{A}_{22} - \boldsymbol{G}\boldsymbol{A}_{12})\,\hat{\boldsymbol{\psi}}_{\boldsymbol{r}}' + (\boldsymbol{A}_{21} - \boldsymbol{G}\boldsymbol{A}_{11})\,\boldsymbol{i}_{\boldsymbol{s}} - \boldsymbol{G}\boldsymbol{B}_1\boldsymbol{u}_{\boldsymbol{s}} + \boldsymbol{G}\frac{\mathrm{d}}{\mathrm{d}t}\boldsymbol{i}_{\boldsymbol{s}} \tag{10}$$

where $\wedge$ means the estimated values and $\boldsymbol{G}$ is the observer gain matrix. The proposed gain matrix choice is the so called (fixed poled position which, fixing the poles position in spite of the rotor speed, reveals particularly suitable for sensorless control [23].

6.2 MCA EXIN + speed estimation

The MCA EXIN + ROO based speed estimation derives from a modification of the complete state equations of the induction motor [23] so that it exploits the two first scalar equations to estimate the rotor speed, as shown below in discrete form for digital implementation (see (11))

where T_s is the sampling time of the control algorithm and k is the current time sample. See [23] for full explanation of the MCA EXIN + ROO and the precise adopted nomenclature. Equation (11) can be rewritten in the form $\boldsymbol{A}\boldsymbol{x} \simeq \boldsymbol{b}$, where $\boldsymbol{A}$ is called 'data matrix' (which is a vector in the problem at hand), while $\boldsymbol{b}$ is called 'observation vector'. This matrix equation can be solved for $\hat{\omega}_\mathrm{r}$ by using Least-Squares techniques. In particular in literature there exist three Least-Squares techniques, that is, the ordinary least-squares (OLS), the TLS) and the data least-squares which arise when errors are, respectively, present only in $\boldsymbol{b}$ or both in $\boldsymbol{A}$ and in $\boldsymbol{b}$ or only in $\boldsymbol{A}$. In this case, because of modelling errors (uncorrect knowledge of the parameter a_{12} depending on the machine electrical parameters and consequent wrong flux estimation) and possible noise on signals the TLS technique has been chosen; in particular the

Table 2 Parameters of the induction motor

rated power P_{rated}, kW	2.2
rated voltage U_{rated}, V	220
rated frequency f_{rated}, Hz	50
pole-pairs	2
stator resistance R_s, Ω	2.9
stator inductance L_s, mH	223
rotor resistance R_r, Ω	1.52
rotor inductance L_r, mH	229
3-phase magnetising inductance L_m, mH	217
moment of inertia J, kg·m^2	0.0048

Therefore a TLS technique should be used instead of OLS technique. The TLS EXIN neuron is the only neural network capable to solve a TLS problems recursively on-line. In this work, a new generalised Least-Squares technique, the MCA EXIN + (minor component analysis) neuron, is used to compute the rotor speed. This technique is a further improvement of the TLS EXIN neuron [23] and is explained below. Fig. 3 shows the block diagram of the MCA EXIN + reduced order speed observer.

7 Test set-up

The employed test set up consists of two parts, respectively, the grid side and machine side one. The grid side part is composed of the following items:

- A 8 kVA, three-phase VSI.
- A dSPACE card (DS1103) with for the control of the grid side inverter.

The machine side part is composed of the following items:

- A three-phase induction motor with parameters shown in Table 2.
- A 8 kVA, three-phase VSI for the control of the machine side inverter.

$$\begin{bmatrix} a_{12}\,T_\mathrm{s}\,\hat{\psi}_{rq}(k-1) \\ -a_{12}\,T_\mathrm{s}\,\hat{\psi}_{rd}(k-1) \end{bmatrix} \hat{\omega}_\mathrm{r}(k-1)$$
$$= \begin{bmatrix} i_{sD}(k) - i_{sD}(k-1) - a_{11}\,T_\mathrm{s}\,i_{sD}(k-1) - a_{12}\,p_\mathrm{r}\,T_\mathrm{s}\,\hat{\psi}_{rd}(k-1) - b\,T_\mathrm{s}\,\hat{u}_{sD}(k-1) \\ i_{sQ}(k) - i_{sQ}(k-1) - a_{11}\,T_\mathrm{s}\,i_{sQ}(k-1) - a_{12}\,p_\mathrm{r}\,T_\mathrm{s}\,\hat{\psi}_{rq}(k-1) - b\,T_\mathrm{s}\,\hat{u}_{sQ}(k-1) \end{bmatrix} \tag{11}$$

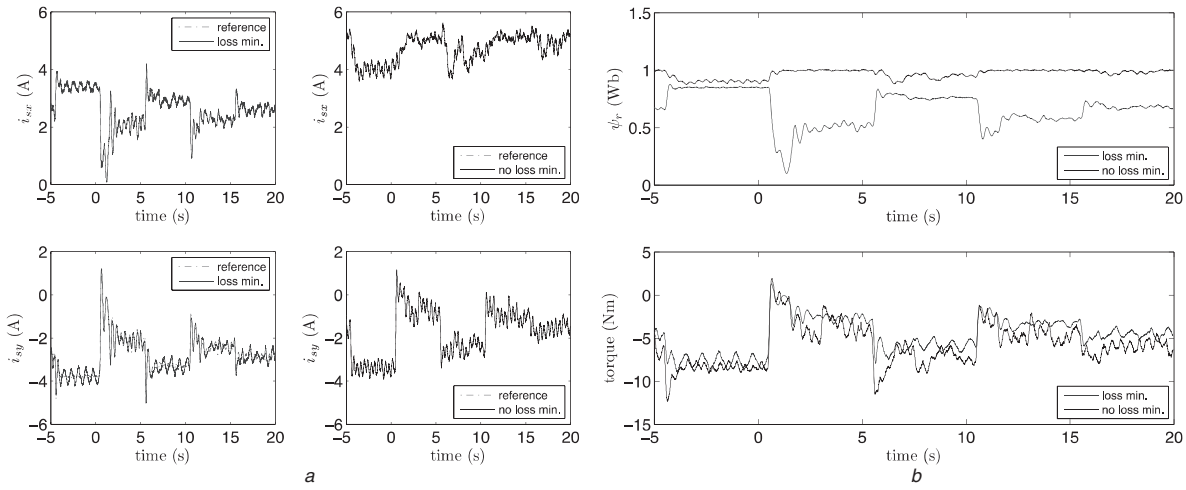

Fig. 6 *Block diagram of the MCA EXIN + reduced order speed observer*

a Machine side i_{sx}, i_{sy} reference and measured currents, with and without ELMT (left-hand side)
b Machine side reference and estimated rotor flux ψ_r and torque t_e, with and without ELMT (right-hand side)

- A brushless interior mounted permanent magnets machine drive for emulating the wind turbine.
- A dSPACE card (DS1103) for the control of the machine side inverter.

Figs. 4*a* and *b* show two photographs of the test setup. To properly emulate experimentally the wind turbine behaviour in each working condition in a laboratory framework, the wind turbine has been substituted by a torque controlled PMSM drive. The PMSM drive receives in input the torque reference on the basis of the turbine model (see Section 2), which has as inputs the wind speed (given by the user) and the machine rotational speed (given by the incremental encoder connected to the shaft). In this way, the PMSM machine drive behaves exactly as the wind turbine for each value of the wind speed and the machine speed.

8 Experimental results

The proposed IM-based wind generator with integrated GNG-based MPPT, ELMT, D-PWM and MCA EXIN + ROO speed estimation has been tested experimentally on the test set-up described in Section 7. To demostrate how much the generated power and energy can be augmented thanks to the integration, besides the MPPT, also of the ELMT and the D-PWM, all the tests in the following have been performed twice, respectively, adopting only the MPPT and then integrating it with ELMT plus D-PWMmax. In both cases, the speed control loop has been closed adopting the speed estimated by the MCA EXIN + ROO.

The wind generation system, initially working in steady-state at the free wind speed of 5.5 m/s, has been given the following set of wind speeds: 3.7, 5, 4 and 4.5 m/s.

Fig. 5*a* shows the real wind speed (red) and the corresponding estimated by the GNG network, with the adoption of ELMT + D-PMW (black) and without it (blue). It should be observed that the estimated speed suitably tracks the real one for each value of the wind speed, in both cases. A slight improvement of the wind speed estimation accuracy is to be noted, when the ELMT + D-PMW are adopted, which is however negligible from the point of view of the final system performance.

Correspondingly to the above wind speed variations, Fig. 5*b* shows the reference, the measured and the estimated IM speed. The higher is the wind speed, the higher is the IM rotating speed, according to the logic of MPPT. Moreover, the IM speed estimated by the MCA EXIN + ROO very well tracks the measured one, for every value of the wind speed, confirming the reliability of the IM speed estimation in such an application for any value of the turbine torque (disturbance of the speed observer). Fig. 6*b* shows the IM reference and estimated rotor flux amplitude as well as the estimated electromagnetic torque. It can be observed that, in case of ELMT + D-PWM, the reference rotor flux varies as expected: in details, the lower is the wind speed, the lower of the toque of wind turbine, the lower is the reference flux needed to cope with the turbine torque, while minimising the IM losses. With regard to the torque waveforms, it can be observed that, the higher is the wind speed, the higher is the amplitude electromagnetic torque at MPP, as expected.

Fig. 6*a* shows the corresponding machine direct and quadrature, reference and measured current components i_{sx}, i_{sy}. Coherently with results in Fig. 6*b*, with the adoption of ELMT + D-PWM i_{sx} varies accordingly to the wind speed variations. On the contrary, without the adoption of ELMT + D-PWM, i_{sx} remains constant to the level corresponding to the rated rotor flux. With regard to i_{sy}, with and without the adoption of ELMT + D-PWM, it shows a reduction of the amplitude for each increase of the motoring torque of the turbine.

Figs. 7*a* and *b* show, respectively, the grid side i_{sd}, i_{sq} reference and measured currents and the active (P) and reactive (Q) power flowing into the power grid, respectively, with and without ELMT + D-PWM. They show that both the i_{sq} current and reactive power Q are controlled to zero, showing that no reactive power exchange with the power grid exists. On the contrary, increases (decreases) of both the i_{sd} current and the active power P occur in accordance with the increases (decreases) of the estimated wind speed. It should be noted that, while there is basically no difference in reactive power control flow (i_{sq} current component) between the case of adopting ELMT + D-PWM and not adopting it, a significant difference exists in terms of active power flow. As a matter of fact there is a significant increase of the active power injected into the power grid with the adoption of ELMT + D-PWM, with respect to the case of not adopting it: the lower is the wind speed, the higher is this increase. The amount of the average active power injected into the power grid against the wind speed is shown in Table 3. It can be observed that, while at the wind speed of 5.5 m/s, the achievable per cent power increase is very small, which is to be expected because the IM works close to its rated speed and torque and thus the ELMT has limited capability to reduces its losses, at wind speed of 3.7 m/s the increase of power is almost 200%. In this last case, if the ELMT + D-PWM is not adopted, the wind generator absorbs from the power grid almost 100 W, with the IM behaving as a motor instead of behaving as a generator: in this conditions, the overall losses are higher than the generable power from the IM and therefore the power balance to the grid is negative. On the contrary, under the same working conditions, the adoption of ELMT + D-PWM permits the system to inject into the power grid almost 100 W, with per cent increase in the injected power of almost

IET Control Theory Appl., 2015, Vol. 9, Iss. 12, pp. 1831–1838

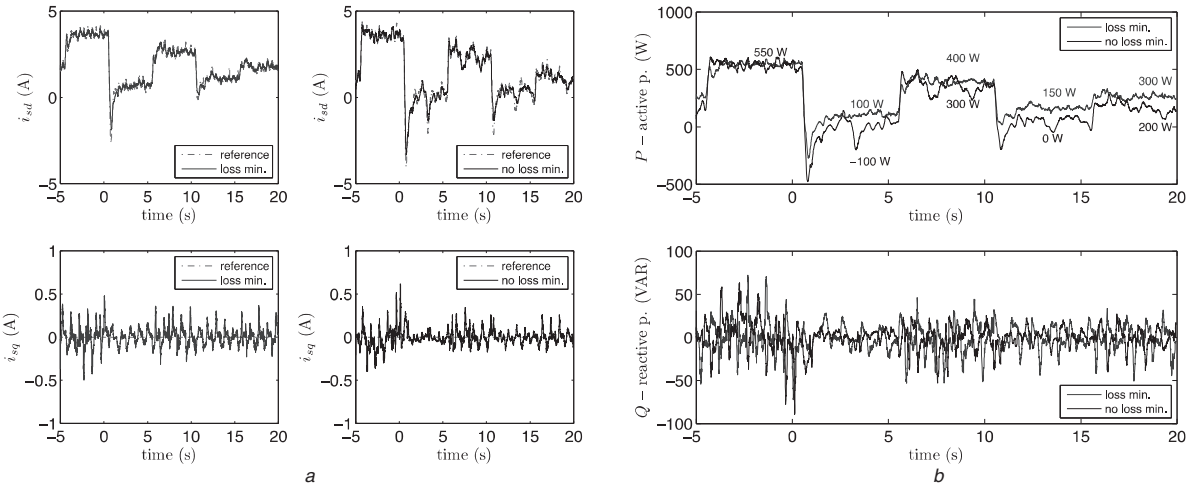

Fig. 7 *Reference and measured currents, with and without ELMT*

a Grid side i_{sd}, i_{sq} reference and measured currents, with and without ELMT (left-hand side)
b Active (P) and reactive (Q) power flowing to the power grid, with and without ELMT (right-hand side)

Table 3 Parameters of the induction motor

Wind speed, m/s	ΔP, %
3.7	200
4	150
4.5	25
5	35
5.5	/

200%. These values confirm that the integration of the ELMT + D-PWM with the MPPT permits a significant increase of the generated power, and in particular a far better exploitation of the low values of the wind speed, which are those statistically more frequent.

Fig. 8*a* shows the torque against speed characteristics of the adopted wind turbine for the tested values of the wind speed (3.7, 4, 4.5, 5, 5.5 m/s), as well as the steady-state maximum power curve (yellow) and the transient loci described by the turbine torque against the speed, in the case of adopting the ELMT + D-PWM. Two loci have been drawn, showing, respectively, with the measured and estimated IM speed. It should be noted that the steady-state points of both these loci lie very close to the corresponding crossing points between the turbine characteristics and the maximum power trajectory. Moreover, the transient torque locus of the IM obtained with the MCA EXIN + RRO is very close to that obtained with the measured speed, confirming the accuracy of the IM speed estimation even during transients, assessing its goodness in such a task.

Finally, Fig. 12 shows the energy generated by the IM and that injected into the power grid during this test, in case of adopting and not adopting ELMT + D-PWM. It can be seen that the energy generated by the IG with ELMT + D-PWM is 2.5×10^{-3} kWh against 2×10^{-3} kWh obtained without the adoption of ELMT + D-PWM, which corresponds to an increase of 25% of the generated energy. The energy injected into the power grid with ELMT + D-PWM is 2.0×10^{-3} kWh against 1.5×10^{-3} kWh obtained without the adoption of ELMT + D-PWM, which corresponds to an increase of 33% of the injected energy.

9 Conclusions

This paper presents an IM-based wind generation unit with integrated MPPT, ELMT, D-PWM, and MCA EXIN + Reduced Order speed Observer features. It proposes the development of a highly

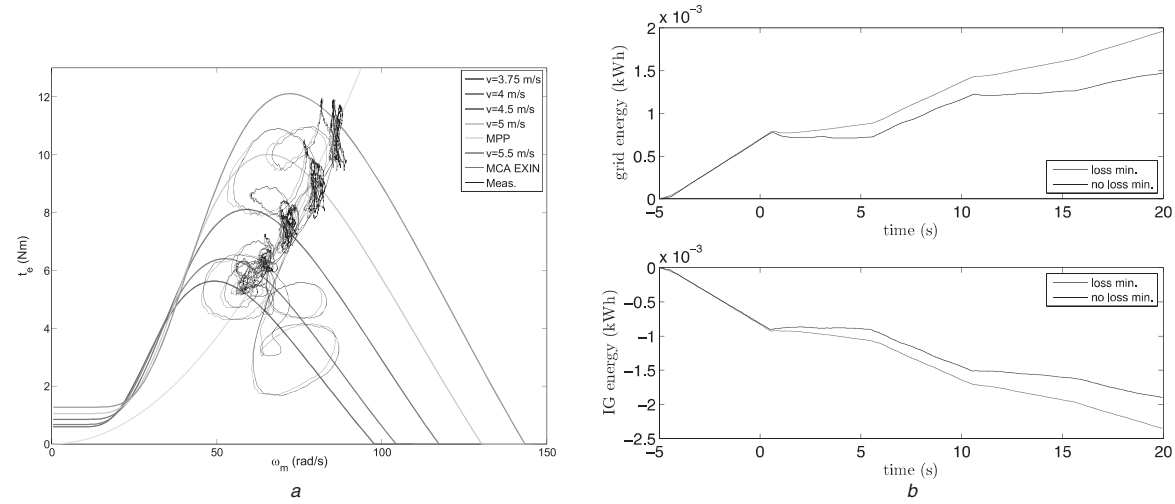

Fig. 8 *Torque against speed characteristics of the adopted wind turbine for the tested values of the wind speed*

a Torque locus and MPPs for different wind speeds, with and without MCA EXIN + ROO (left-hand side)
b Electric energy generated by the machine and injected to the power grid, with and without ELMT (right-hand side)

efficient wind generation unit with high dynamic performance, able not only to track the maximum generable power rapidly according to any wind speed variation, but also to minimise, at the same time, the converter's and the machine's losses. Particularly, the power converters' switching losses have been reduced adopting a D-PWM, while the IM overall losses have been reduced adopting a suitable ELMT. Contemporary, to reduce costs and increase the reliability of the system, it has been devised hence to be a fully sensorless generation unit, meaning that both the wind speed and the machine speed sensors are not present. The real anemometer has been substituted by the wind speed estimator integrated in the MPPT, based on the GNG network. The IM encoder has been substituted with an intelligent speed estimator, the so called MCA EXIN + ROO.

The proposed wind generator is based on a back-to-back power converter topology with two VSI, respectively, one on the machine side and the other on the grid side. The proposed wind generation unit has been tested experimentally on a suitably developed test set-up. Results clearly show that the integration of ELMT + D-PWM into the wind generator control with NN based MPPT, permits the active power injected to the power grid to be increased from 35% at high wind speeds up to 200% at low wind speeds.

10 Acknowledgments

This paper has been funded by the following research projects: RITmare, Ricerca ITaliana per il mare (Italian Research for the sea); TESEO, Tecnologie ad alta Efficienza per la Sostenibilità Energetica ed ambientale On-board (High efficiency technologies for on-board energy and environmental sustainability); CNR per il Mezzogiorno (Advanced Technologies for Energy Efficiency and Sustainable Mobility).

11 References

1 Kazmierkowski, M.P., Krishnan, R., Blaabjerg, F.: 'Control in power electronics' (London, UK, 2002)
2 Simões, M.G., Farret, F.A.: 'Alternative energy systems: design and analysis with induction generators' (CRC Press, 2nd edn.)
3 Chen, Z., Guerrero, J.M., Blaabjerg, F.: 'A review of the state of the art of power electronics for wind turbines', *IEEE Trans. Power Electr*., 1998, **24**, (8), pp. 1859–1874
4 Li, H., Chen, Z.: 'Overview of different wind generator systems and their comparisons', *IET Renew. Power Gener*., 2008, **2**, (2), pp. 123–138
5 Simões, M.G., Bose, B.K., Spiegel, R.J.: 'Fuzzy logic based intelligent control of a variable speed cage machine wind generation system', *IEEE Trans. Power Electr*., 1997, **12**, (1)
6 Simões, M.G., Bose, B.K., Spiegel, R.J.: 'Design and performance evaluation of a fuzzy-logic-based variable-speed wind generation system', *IEEE Trans. Ind. Appl*., 1997, **33**, (4)
7 Koutroulis, E., Kalaitzakis, K.: 'Design of a maximum power tracking system for wind-energy-conversion applications', *IEEE Trans. Ind. Electron*., 2006, **53**, (2)
8 Thiringer, T., Linders, J.: 'Control by variable rotor speed of a fixed-pitch wind turbine operating in a wide speed range', *IEEE Trans. Energy Convers.*, 1993, **8**, (3), pp. 520–526
9 Senjyu, T., Ochi, Y., Muhando, E., Urasaki, N., Sekine, H.H.: 'Speed and position sensor-less maximum power point tracking control for wind generation system with squirrel cage induction generator'. Power Systems Conf. and Exposition, 2006 (PSCE '06), October 29–November 1 2006, pp. 2038–2043
10 Uctug, M.Y., Eskandarzadeh, I., Ince, I.H.: 'Modelling and output power optimisation of a wind turbine driven double output induction generator', *IEE Proc. Electr. Power Appl.*, 2004, **41**, (2), pp. 33–38
11 Karrari, M., Rosehart, W., Malik, O.P.: 'Comprehensive control strategy for a variable speed cage machine wind generation unit', *IEEE Trans. Energy Convers*., 2005, **20**, (2), pp. 415–423
12 Shao, C., Chen, X., Liang, Z.: 'Application research of maximum wind-energy tracing controller based adaptive control strategy in WECS'. Power Electronics and Motion Control Conf. 2006 (IPEMC '06), August 2006, vol. 1, pp. 1–5
13 Shi, K.L., Li, H.: 'A novel control of a small wind turbine driven generator based on neural networks'. Power Engineering Society General Meeting, IEEE, 2004
14 Nguyen, D., Hobraiche, J., Patin, N., Friedrich, G., Vilain, J.: 'A direct digital technique implementation of general discontinuous pulse width modulation strategy', *IEEE Trans. Ind. Electron*, 2011, **58**, (9), pp. 4445–4454
15 Holmes, D.G., Lipo, T.A.: 'Pulse width modulation for power converters' (Wiley, 2003)
16 Hava, A.M., Kerkman, R.J., Lipo, T.A.: 'A high performance generalized discontinuous PWM algorithm', *IEEE Trans. Ind. Appl*., 1998, **34**, (5)
17 Kirschen, D.S., Novotny, D.W., Lipo, T.A.: 'Optimal efficiency control of an induction motor drive', *IEEE Trans. Energy Convers.*, 1987, **EC-2**, (1), pp. 70–75
18 Canudas de Wit, C., Seleme, Jr. S.I.: 'Robust torque control design for induction motors: the minimum energy approach', *Automatica*, 1997, **33**, (1), pp. 63–79
19 Mesemanolis, Mademlis, C., Kioskeridis, I.: 'Optimal efficiency control strategy in wind energy conversion system with induction generator', *IEEE J. Emerging Sel. Top. Power Electron.*, 2013, **1**, (4), pp. 238–246
20 Holtz: 'Sensorless control of induction motor drives', *Proc. IEEE*, 2002, **90**, (8), pp. 1359–1394
21 Briz, F., Degner, M.W., Diez, A., Lorenz, R.D.: 'Static and dynamic behavior of saturation-induced saliencies andd their effect on carrier – signal – based sensorless AC drives', *IEEE Trans. Ind. Appl.*, 2002, **38**, (3)
22 Cirrincione, M., Pucci, M., Vitale, G.: 'Power converters and AC electrical drives with linear neural networks', in A. Emadi (Ed.): 'Energy, power electronics, and machines' (Taylor & Francis, New York, NY, USA, 2012, 1st ed.)
23 Cirrincione, M., Pucci, M., Cirrincione, G., Capolino, G.: 'Sensorless control of induction motors by reduced order observer with MCA EXIN + based adaptive speed estimation', *IEEE Trans. Ind. Electron.*, 2007, 54, (1), Special Section Neural Network Applications in Power Electronics and Motor Drives (Guest Editor B.K. Bose)
24 Cirrincione, M., Pucci, M., Vitale, G.: 'Growing neural gas based MPPT of variable pitch wind generators with induction machines', *IEEE Trans. Ind. Appl.*, 2012, **48**, (3), pp. 1006–1016
25 Pucci, M., Cirrincione, M.: 'Neural MPPT control of wind generators with induction machines without speed sensors', *IEEE Trans. Ind. Electron.*, 2011, **58**, (1), Special Section Renewable Energy Systems
26 Pucci, M.: 'Sensors-less neural maximum power point tracking control of induction machines wind generators by growing neural gas and minor component analysis EXIN + reduced order observer', *IET Control Theory Appl.*, 2010, **4**, (9), pp. 1627–1638